RSC Advances

PAPER

View Article Online
View Journal | View Issue

Cite this: *RSC Adv.*, 2022, **12**, 4437

Carbazole-based bis-imidazole ligand-involved synthesis of inorganic–organic hybrid polyoxometalates as electrochemical sensors for detecting bromate and efficient catalysts for selective oxidation of thioether†

Xiang Wang,* Jiafeng Lin, Huan Li, Chenying Wang and Xiuli Wang*

Received 6th December 2021
Accepted 27th January 2022

DOI: 10.1039/d1ra08861k

rsc.li/rsc-advances

Considering the potential application on preparing electrode and catalyst materials of inorganic–organic hybrid polyoxometalates, a bis-imidazole ligand with carbazole as a connector, 3,6-di(1H-imidazol-1-yl)-9H-carbazole (L), was used for preparing inorganic–organic hybrid polyoxometalates. As a result, three complexes formulated by $[NiL_2(Mo_2O_7)]$ (**1**), $[Cu(H_2O)_2(HL)_2\ (\beta\text{-}Mo_8O_{26})]\cdot H_2O$ (**2**) and $[Ni_2(H_2O)_4L_2(CrMo_6(OH)_5O_{19})]\cdot 6H_2O$ (**3**) were obtained successfully. Structural analysis indicated that the different polyoxoanions and metal ions showed important influences on the formation of structures. In the presence of Ni^{2+} ions and heptamolybdate, a 2D network constructed from Ni^{2+} ions and L ligands was formed in complex **1**, in which the $[Mo_4O_{14}]^{4-}$ polyoxoanions were encapsulated. But the use of Cu^{2+} ions led to a 1D chain of complex **2**, which was composed of $[\beta\text{-}Mo_8O_{26}]^{4-}$ polyoxoanions and mononuclear $\{CuL_2\}$ units. By utilizing $[CrMo_6(OH)_5O_{19}]^{4-}$ as the inorganic building block, complex **3** showed a 2D (4, 4)-connected layer. Complexes **1–3** could be employed as electrode materials for sensing bromate with the limits of detection of 0.315 μM for **1**, 0.098 μM for **2** and 0.551 μM for **3**. Moreover, these complexes showed efficient catalytic activity for the selective oxidation of thioethers.

Introduction

Nowadays, polyoxometalates (POMs) as anionic metal oxide clusters have attracted more and more attention because of their satisfactory properties and potential applications in many fields due to excellent redox properties, such as electrochemistry,[1] catalysis,[2,3] energy storage and battery,[4–6] and so on, and also their diverse architectures,[7,8] including classical Keggin, Wells–Dawson, Anderson, Waugh and Lindquist types. However, their disadvantages, such as aggregation and instability in most solvents, often hinder their promising application. Many strategies to overcome these disadvantages have been exploited. For example, the use of a host material is usually considered as a helpful approach, such as carbon nanotubes,[9] or polypyrroles,[10] because they can strengthen the stability of the structure, as well as conductivity and energy density of materials.

Another method is to combine a POM and metal–organic framework (MOF), because MOFs own usually not only high crystallinity and satisfying stability, especially these obtained from hydrothermal condition, but also porous structures featuring 2D or 3D networks resulting from organic ligands as linkers and metal ions, as well as secondary building units, in which the POMs acting as guest molecules or inorganic linkages are involved.[11,12] For instance, the Keggin type POMs as guest molecules were successfully embraced in the porous Cu^{2+}/1,3,5-tricarboxybenzene MOF.[13,14] The N-donor ligands are also popular candidates, because their abundant configurations and linking modes with metal centers usually result in the stable frameworks to accommodate POMs. To this day, a plenty of N-donor ligands have been employed to react with metal ions and POMs under hydrothermal condition, resulting in POM-based complexes materials with excellent properties and structures, where the POMs play different roles in the final structures. For example, the use of metalloporphyrin ligand generated stable POM-based MOFs with remarkable performance for scavenging of dyes and for heterogeneous selective oxidation of alkylbenzenes, or highly selective electroreduction of CO_2.[15–18] The carbazole-contained ligands, 4-{[4-(9H-carbazol-9-yl)phenyl] ethynyl}aniline and 2-(9H-carbazol-9-yl)-N-(1,3-dihydroxy-2-(hydroxymethyl) propan-2-yl)acetamide have been also designed and used to prepare the complexes based on Lindqvist

Liaoning Professional Technology Innovation Center of Liaoning Province for Conversion Materials of Solar Cell, College of Chemistry and Materials Engineering, Bohai University, Jinzhou, 121000, P. R. China. E-mail: xwang@bhu.edu.cn; wangxiuli@bhu.edu.cn

† Electronic supplementary information (ESI) available: Table of bond lengths and angles, PXRD, FTIR, EIS spectra, SEM and Table summarizing sensors of Cr(VI). CCDC [2123433–2123435]. For ESI and crystallographic data in CIF or other electronic format see DOI: 10.1039/d1ra08861k

and Anderson POMs, the non-linear optical property and genotoxicity of which were evaluated.[19,20]

Based on their potential feasibilities of the analysis of the electrocatalytic reaction,[21] the electrochemical techniques were regarded as considerable means for detecting bromate because of their high sensitivity, uncomplicated and fast procedures,[22] compared with other ways such as ion chromatography,[23] liquid chromatography-mass spectrometry,[24] spectrofluorometry,[25] and so on. The POM-based complexes may be satisfactory candidates as electrode materials to prepare the electrochemical sensor for detecting bromate due to their stable structures and satisfactory redox abilities. For example, the complexes based on Keggin and Wells–Dawson POMs by using 1,4-bis(1-imidazol-yl)-2,5-dimethyl benzene, 1,2,4-triazole and terphenyl-based tricarboxylate as organic ligands, could be chosen as electrode materials to fabricate electrochemical sensors for the detection of bromate.[26–28] The complexes based on octamolybdate and Anderson POMs originated from bis-amide ligands exhibited promising applications on the preparation of electrochemical sensors of bromate.[29,30] Further, such complexes could also be utilized to prepare composite materials or films as the electrode materials of electrochemical sensors of bromate.[31–33] The above investigations manifest that the synthesis of polyoxometalate-based complexes composed of metal ions and organic ligands is of great significance for the development of catalysts and electrode materials.

In this work, a bi-imidazole ligand bridged each other by a carbazole connector, 3,6-di(1H-imidazol-1-yl)-9H-carbazole(L), was used in order to synthesize the POM-based complex materials. By adjusting the polyoxoanions and metal ions, three POM-based complexes, $[NiL_2(Mo_2O_7)]$ (**1**), $[Cu(H_2O)_2(HL)_2(\beta\text{-}Mo_8O_{26})]\cdot H_2O$ (**2**) and $[Ni_2(H_2O)_4L_2(CrMo_6(OH)_5O_{19})]\cdot 6H_2O$ (**3**), have been prepared under hydrothermal condition. Complex **1** is a 2D structure, and the $[Mo_4O_{14}]^{4-}$ inorganic units are encapsulated in a network constructed from Ni^{2+} ions and L ligands. Complex **2** shows a chilopod-like chain composed of mononuclear $\{CuL_2\}$ units and $[\beta\text{-}Mo_8O_{26}]^{4-}$ polyoxoanions. In **3**, the L ligands link the 1D $[CrMo_6(OH)_5O_{19}]^{4-}$ POM-based inorganic chains into a 2D (4,4)-connected network. The metal centers and polyoxoanions play important roles in tuning the diverse architectures. Moreover, the complexes display satisfying electrochemical sensing behaviors for BrO_3^- and catalytic performance for oxidation of thioether to sulfoxide.

Experimental

Reagent and apparatus

The L ligand and other reagents during experimental operation were purchased from commercial sources and used directly. FT-IR were measured on a Varian 640 FT-IR spectrometer (KBr pellets). The morphological characterization was analysed by using a Hitachi S-4800 scanning electron microscope (SEM). The powder X-ray diffraction (PXRD) data was collected by using a Rigaku Ultima IV diffractometer. The catalytic reaction of oxidation of thioether was monitored by utilizing a Shimadzu Techcomp GC-7900.

Preparation of complexes 1–3

Synthesis $[NiL_2(Mo_2O_7)]$ (1). A mixture of $Ni(CH_3COO)_2\cdot 4H_2O$ (0.05 g, 0.2 mmol), L (0.012 g, 0.04 mmol) and $(NH_4)_6Mo_7O_{24}\cdot 4H_2O$ (0.05 g, 0.04 mmol) in 10 mL deionized water was stirred for 1 hour. After the pH was adjusted to 4.9 with 0.1 M HCl and NaOH, which was transferred into a 25 mL Teflon-lined autoclave and reacted successively at 160 °C for 4 days. Green crystals were isolated. Yield: 63% (based on Ni). IR (solid KBr pellet, cm^{-1}): 1611(w), 1582(s), 1511(s), 1466(m), 1396(m), 1270(s), 1255(m), 968(w), 908(s), 807(s), 732(s).

Synthesis of $[Cu(H_2O)_2(HL)_2(\beta\text{-}Mo_8O_{26})]\cdot H_2O$ (2). The method was similar to that of complex **1**, except the $Ni(CH_3COO)_2\cdot 4H_2O$ was replaced with $CuCl_2\cdot 2H_2O$ (0.034 g, 0.2 mmol). Green crystals were isolated. Yield: 53% (based on Cu). IR (solid KBr pellet, cm^{-1}): 3434(w), 1614(w), 1586(w), 1528(s), 1468(w), 1400(m), 1270(s), 1252(s), 951(s), 905(s), 838(s), 725(s).

Synthesis $[Ni_2(H_2O)_4L_2(CrMo_6(OH)_5O_{19})]\cdot 6H_2O$ (3). The method was similar to that of complex 1, except the $(NH_4)_6Mo_7O_{24}\cdot 4H_2O$ was replaced with $Na_3[CrMo_6O_{24}H_6]\cdot 8H_2O$ (0.06 g, 0.048 mmol), and the reaction temperature is 120 °C. Green crystals were isolated. Yield: 48% (based on Ni). IR (solid KBr pellet, cm^{-1}): 3499(w), 1610(s), 1538(s), 1467(w), 1429(s), 1248(s), 943(s), 905(s), 842(m), 804(m), 737(m), 654(m).

Electrochemical measurements

All electrochemical studies were achieved on a CHI 660 electrochemical workstation. The cyclic voltammogram and amperometric measurements were performed to study the response current and sensing behavior toward bromate of the electrode materials prepared from three complexes. Electrochemical measurements were performed in 0.1 M H_2SO_4 + 0.5 M Na_2SO_4 aqueous solution containing a certain number of bromate. The carbon paste electrodes (CPEs) modified by complexes **1–3** (**1–3**-CPEs),[34] Pt wire and saturated calomel electrode were chosen as the working, counter and reference electrodes.

General procedure for the oxidation of sulfides

Sulfides (0.5 mmol), *tert*-butyl hydroperoxide (TBHP) (0.75 mmol), catalyst (3 μmol), and methanol (2 mL) were added into a 25 mL round-bottom tube. The mixture was reacted at the set temperature. The conversion and selectivity of the resulting products were analyzed by GC with naphthalene as an internal standard.

X-ray structure determination

The crystal data of complexes **1–3** were collected on a Bruker SMART APEX II with Mo $K\alpha$ ($\lambda = 0.71073$ Å) at 293 K by ω and θ scan mode. All structures of **1–3** were solved and refined by employing SHELXTL-2014 packages and Olex2 software and using direct methods.[35,36] The primary crystal data and structure refinements of **1–3** are summarized in Table 1. The crystallographic data of **1–3** have been deposited in the Cambridge Crystallographic Data Center with CCDC No. 2123433–2123435. Table S1† includes the selected bond lengths and angles.

Table 1 Crystal data and structure refinement for complexes **1–3**

Complex	**1**	**2**	**3**
Formula	$C_{36}H_{26}Mo_2N_{10}NiO_7$	$C_{36}H_{34}CuMo_8N_{10}O_{29}$	$C_{36}H_{51}CrMo_6N_{10}Ni_2O_{34}$
F_w	961.24	1901.77	1912.86
Crystal system	Monoclinic	Monoclinic	Triclinic
Space group	$P2_1/n$	$C2/c$	$P\bar{1}$
a Å^{-1}	12.1311 (14)	8.4459 (4)	7.8269 (4)
b Å^{-1}	19.995 (2)	24.3390 (11)	10.4537 (5)
c Å^{-1}	14.5390 (16)	24.7639 (11)	17.1966 (8)
α °$^{-1}$	90.000 (5)	90	95.1090 (10)
β °$^{-1}$	93.938 (2)	95.4410 (10)	91.5670 (10)
γ °$^{-1}$	90.000 (5)	90	97.2660 (10)
V Å^{-3}	3518.2 (7)	5067.6 (4)	1389.12 (12)
Z	4	4	1
D_c (g cm^{-3})	1.815	2.487	2.261
μ mm^{-1}	1.299	2.427	2.264
F (000)	1920.0	3652.0	920.0
Final R_1,[a] wR_2[b] [$I > 2\sigma(I)$]	0.0490, 0.1303	0.0355, 0.0721	0.0383, 0.0908
Final R_1,[a] wR_2[b] (all data)	0.0813, 0.1552	0.0623,0.0810	0.0524, 0.0974
Goodness on F^2	0.918	1.017	1.042

[a] $R_1 = \sum||F_o| - |F_c||/\sum|F_o|$. [b] $wR_2 = [\sum w(F_o^2 - F_c^2)^2]/\sum[w(F_o^2)^2]^{1/2}$.

Results and discussion

Crystal structures

Complex **1** consists of one Ni^{2+} ion, two L ligands and one $[Mo_2O_7]^{2-}$ anion. Bond valence sum calculation indicates the Ni and Mo ions are in +II and +VI oxidation states,[37] respectively. The Ni atom shows a six-coordinated mode with an octahedral configuration (Fig. 1a), surrounded by two terminal oxygen atoms belonging to $[Mo_2O_7]^{2-}$ anion and four nitrogen atoms from two L ligands. The bond length of Ni–O and Ni–N are 2.056–2.192 Å. All two Mo atoms are five-coordinated modes. Both $\{MoO_2\}$ and $\{MoO_3\}$ clusters are aggregated through one bridged oxygen atom μ_2-O7 to form a $\{Mo_2O_6\}$ cluster (Fig. 1b). Two μ_3-O6 oxygen atoms connect two $\{Mo_2O_6\}$ clusters into a $\{Mo_4O_{14}\}$ cluster (Fig. 1c).

Complex **1** is a 2D structure. Firstly, a binuclear metal–organic ring $\{Ni_2L_2\}$ with a size of 11.58 Å × 9.90 Å is constructed from two Ni atoms and two L ligands depending on the coordination bonds between imidazole group and Ni atom (Fig. 2a). The size of the $\{Ni_2L_2\}$ ring is enough to accommodate one $\{Mo_4O_{14}\}$ cluster, in which one $\{Mo_4O_{14}\}$ cluster can be perfectly encapsulated, resulting in a POM-based ring. Moreover, the $\{Mo_4O_{14}\}$ cluster provides two pairs of oxygen atoms including two terminal O5 and two μ_2-O7 atoms to coordinate together with the Ni atoms from the $\{Ni_2L_2\}$ ring (Fig. 2b), respectively. Further, the remaining L ligand links the POM-based ring into a 2D layer (Fig. 2c), which offers two N atoms of imidazole group to coordinated with the Ni atom from adjacent POM-based ring. In fact, each of Ni atoms of the POM-based ring is surrounded by four L ligand. Or to say, the $\{Ni_2L_2\}$ rings are extended *via* four L ligands into a 2D network and the $\{Mo_4O_{14}\}$ cluster are embedded into these $\{Ni_2L_2\}$ rings. Considering the POM-based rings as four connected modes, the 2D layer can be simplified as a (4, 4)-connected network (Fig. 2d).

Complex **2** is compose of one Cu^{2+} ion, one $[\beta\text{-}Mo_8O_{26}]^{4-}$ (abbreviated to Mo_8) polyoxoanion, two L ligands, two coordinated water molecules and one crystal water molecule. One of two imidazole groups of L ligand is protonated. Bond valence sum calculation indicates the Cu and Mo ions are in +II and +VI oxidation states,[37] respectively. The Cu atom has a six-coordinated mode (Fig. 3a), defined by two nitrogen atoms from two L ligands, two oxygen atoms of the Mo_8 anion and two water molecules. The bond length of Cu–O and Cu–N are 1.951–2.303 Å.

In the structure of complex **2**, the combination of two L ligands and one Cu atom *via* Cu–N coordination bond to generate a mononuclear unit $\{CuL_2\}$ (Fig. 3b). Each of Mo_8 polyoxoanions acting as bidentate inorganic building block utilizes two symmetric terminal oxygen atoms to coordinate with the Cu atom from the mononuclear unit $\{CuL_2\}$, forming a 1D chilopod-like chain of complex **2** (Fig. 3c). Meanwhile, two water molecules compensate the coordination numbers of the Cu center.

Complex **3** consists of one Ni^{2+} ion, two L ligands, one Anderson-type polyoxoanion $[CrMo_6(OH)_5O_{19}]^{4-}$ (abbreviated to $CrMo_6$), three coordinated water molecules and six crystal water molecules. Bond valence sum calculation indicates the Ni and Mo ions are in +II and +VI oxidation states,[37] respectively.

The six-coordinated Ni atom is surrounded by two water molecules, two nitrogen atoms from two imidazole groups of L ligand, two oxygen atoms of the $CrMo_6$ anion (Fig. 4a), showing an octahedral configuration. The $CrMo_6$ anion acts as a tetradentate inorganic ligand to provide four oxygen atoms to coordinate with four Ni atoms.

Complex **3** has a 2D structure. The Ni atoms join the $CrMo_6$ anions in pairs into a 1D POM-based inorganic chain (Fig. 4b). Then the L ligand plays a role of bi-dentate linker, utilizing two nitrogen atoms of imidazole group to coordinate with two Ni atoms from neighboring POM-based inorganic chains. Such the

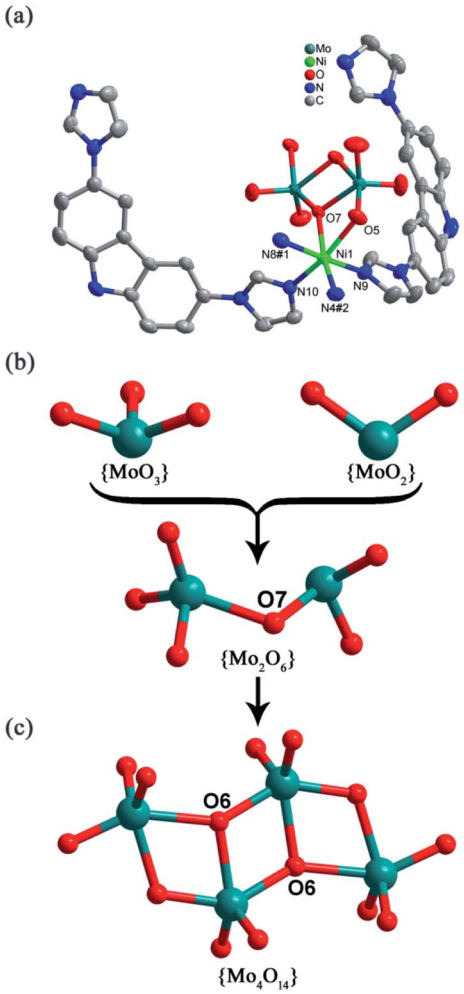

Fig. 1 (a) View of crystal structure of **1** (50% thermal ellipsoids). All hydrogen atoms are omitted for clarity. #1: $1-x, 1-y, 1-z$; #2: $1.5-x, 0.5+y, 0.5-z$. (b) View of the $\{Mo_2O_6\}$ cluster. (c) View of the $\{Mo_4O_{14}\}$ cluster.

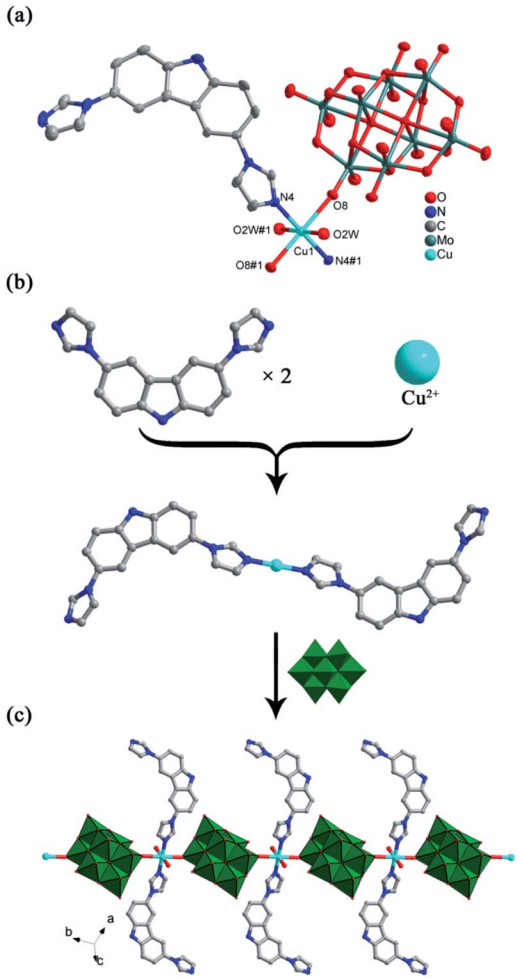

Fig. 3 (a) View of crystal structure of **2** (50% thermal ellipsoids). All hydrogen atoms and crystal water molecules are omitted for clarity. #1: $-x, 1-y, 1-z$. (b) View the mononuclear $\{CuL_2\}$ composed of two L ligands and one Cu center. (c) The chilopod-like 1D chain of complex **2**.

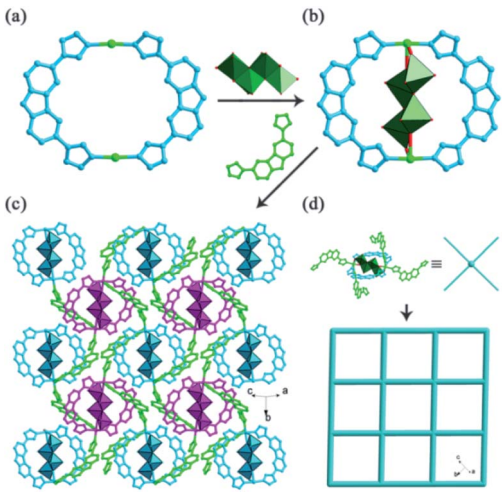

Fig. 2 (a) View of the metal–organic ring $\{Ni_2L_2\}$. (b) The $\{Mo_4O_{14}\}$ cluster-encapsulated ring. (c) View of the 2D layer of complex **1**. (d) View of the (4, 4)-connected network of **1**.

coordination pattern induces a 2D structure of complex **3**. If both Ni atoms and $CrMo_6$ anions are considered as four-connected nodes, the 2D layer can be simplified as a (4,4)-connected network (Fig. 4c).

Morphology, PXRD and FT-IR spectra

The SEM of the crystalline complexes was carried out, as shown in Fig. S1.† It can be observed that the lumpy crystals of complexes **1–3** were synthesized during their preparation process. The phase purity of complexes **1–3** was verified by PXRD. The experimental diffraction peaks are consistent with that simulated by crystal data, as shown in Fig. S2,† revealing that two complexes have good phase purities. Additionally, the IR spectra of **1–3** and L were recorded in the range of 4000–400 cm^{-1} (Fig. S3†). The absorption bands in the region of 1582 to 1062 cm^{-1} indicate the presence of organic ligand L. The absorption bands at 929, 908, 880, 807 cm^{-1} for **1**, 955, 904,836, 817 cm^{-1} for **2**, 938, 918, 885, 634, 568 cm^{-1} for **3**, should be

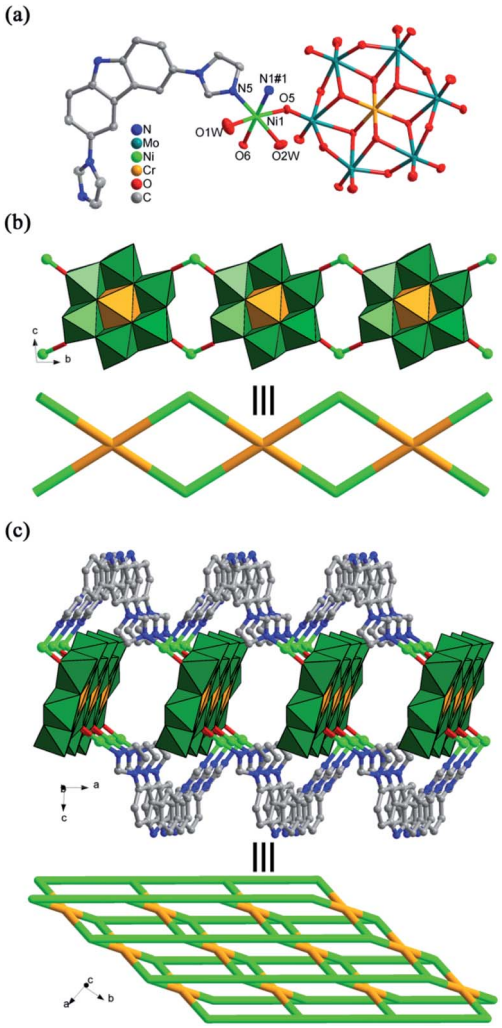

Fig. 4 (a) View of crystal structure of **3** (50% thermal ellipsoids). All hydrogen atoms and crystal water molecules are omitted for clarity. #1: $-1 + x, 1 + y, z$. (b) The POM-based inorganic chain constructed from Ni atoms and $CrMo_6$ anions. (c) View of the 2D layer of complex **3**.

ascribed to the characteristic peaks of polyoxoanions.[30,38] These results confirm further the composition of all three complexes.

Electrochemical properties

The electrochemical properties of complexes **1–3**, including the cyclic voltammogram, electrocatalytic and amperometric sensing behaviors, were investigated. As shown in Fig. 5a–c, three complexes show three pairs of redox peaks with the average peak potentials calculated based on $E_{1/2} = (E_{pa} + E_{pc})/2$ of +284 mV (I–I′), +30 mV (II–II′), −160 mV (III–III′) for **1**-CPE, +208 mV (I–I′), +65 mV (II–II′), −146 mV (III–III′) for **2**-CPE, +186 mV (I–I′), +41 mV (II–II′), −99 mV (III–III′) for **3**-CPE, respectively, which should be attributed to three consecutive two-electron redox processes of Mo centers.[39] The linear relationship between peak current and scan rate (II–II′) indicates that the redox reaction belongs to be surface-controlled (Fig. 5d). The excellent redox abilities of complexes **1–3**

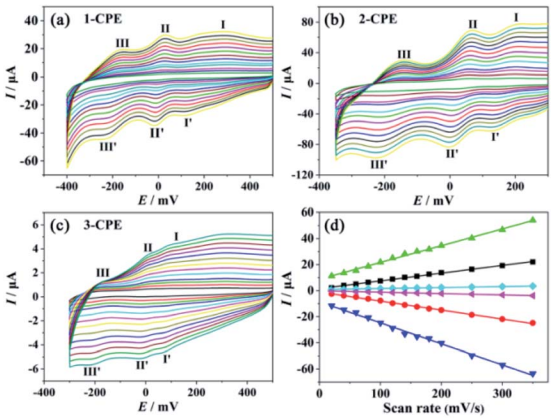

Fig. 5 (a–c) Cyclic voltammograms of **1–3**-CPEs in 0.1 M H_2SO_4 + 0.5 M Na_2SO_4 aqueous solution at different scan rates (from inner to outer: 20, 40, 60, 80, 100, 120, 140, 160, 180, 200, 250, 300 and 350 mV s^{-1}). (d) The plots of the anodic and cathodic peak currents *vs.* scan rates (II–II′).

indicate their potential applications as electrode materials in the electrochemical fields.

Based on the excellent redox abilities of complexes **1–3**, the electrocatalytic activities of **1**-, **2**- and **3**-CPEs toward the reduction of BrO_3^- were inspected in the 0.1 M H_2SO_4 + 0.5 M Na_2SO_4 aqueous solution. It can be observed that the gradual addition of BrO_3^- causes the obvious increase of reduction peak currents of **1–3**-CPEs (Fig. 6a–c), especially the third reduction peak, while the corresponding oxidation peak currents decrease, indicating that complexes **1–3** have good electrocatalytic activities toward the reduction of BrO_3^-, which suggests their potential applications for preparing electrochemical sensors depending on the current responses with the change of concentration.

Further, the electrochemical sensing activities toward BrO_3^- of **1–3**-CPEs as amperometric sensors were evaluated. Fig. 6d–f illustrates that **1–3**-CPEs exhibit quick current responses when the BrO_3^- is added continuously at 30 s intervals at optimal voltage, respectively. At the same time, there is a remarkable linear relationship between response current and substrate concentration in the range of 10 to 1000 μM. Based on the linear regression equation of $I = -8.579C - 0.520$ ($R^2 = 0.998$) for **1**-CPE, $I = -27.614C - 3.807$ ($R^2 = 0.999$) for **2**-CPE and $I = -0.542C + 0.257$ ($R^2 = 0.999$) for **3**-CPE, the sensitivity and limit of detection (LOD) of **1–3**-CPEs are calculated as 8.58 μA mM^{-1} and 0.315 μM for **1**-CPE, 27.61 μA mM^{-1} and 0.098 μM for **2**-CPE, 0.54 μA mM^{-1} and 0.551 μM for **3**-CPE. The LOD of **2**-CPE is lowest in comparison with that **1**-CPE and **3**-CPE, which are comparable to the reported electrochemical sensors (Table S2†). To understand the differences of electrocatalytic activity of the CPEs modified by three complexes, the electrochemical impedance spectroscopy (EIS) could be carried out to determine the electroconductivity of **1–3**-CPEs (Fig. S4†).[40] The Nyquist plot of **2**-CPE possesses smallest charge-transfer impedance than that of **1**- and **3**-CPEs, which may be resulted by their different structures, that may be beneficial to the electron transfer during

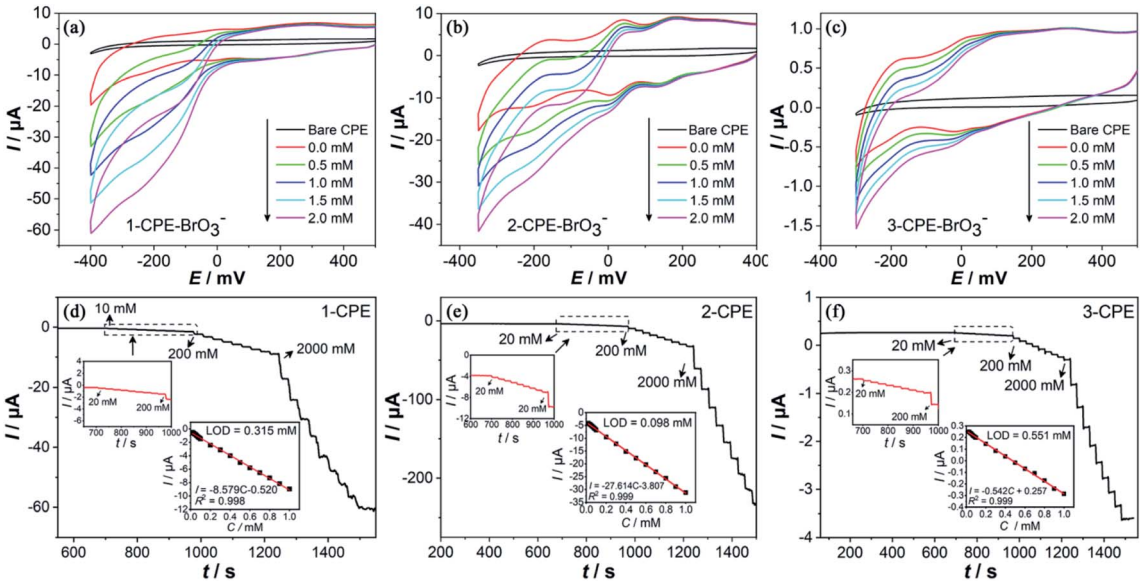

Fig. 6 (a–c) Cyclic voltammograms of **1–3**-CPEs in 0.1 M H_2SO_4 + 0.5 M Na_2SO_4 aqueous solution containing BrO_3^- (scan rate: 60 mV s^{-1}). (d–f) Current responses of **1–3**-CPEs with continuous addition of BrO_3^- per 30 s interval (Inset: the plot of response current *vs.* concentrations of substrate.

the electrocatalytic reduction of BrO_3^-,[40] suggesting the high electrochemical performance of **2**-CPE. The mechanism may be that the BrO_3^- could be reduced by the multi-electron-reduced products of complexes. Three pairs of redox peaks (I–I′, II–II′, III–III′) of **1–3**-CPEs should belong to three consecutive two-electron redox processes of Mo centers, and the electrochemical reaction can be shown as follows.[41,42]

$$\mathrm{POM-complex} + 2\mathrm{H^+} + 2\mathrm{e^-} \rightarrow \mathrm{H_2POM-complex}$$

$$\mathrm{H_2POM-complex} + 2\mathrm{H^+} + 2\mathrm{e^-} \rightarrow \mathrm{H_4POM-complex}$$

$$\mathrm{H_4POM-complex} + 2\mathrm{H^+} + 2\mathrm{e^-} \rightarrow \mathrm{H_6POM-complex}$$

Considering that the addition of BrO_3^- can lead to the obvious increase of reduction peak currents (II–II′, III–III′), especially the third reduction peak, so the catalytic behavior toward BrO_3^- may involve the four-electron-reduced and six-electron-reduced products, producing bromide as the product.[26,43] The catalytic chemical steps can be explained by the following reactions.

$$3\mathrm{H_4POM-complex} + 2\mathrm{BrO_3^-} \rightarrow 3\mathrm{POM-complex} + 2\mathrm{Br^-} + 6\mathrm{H_2O}$$

$$\mathrm{H_6POM-complex} + \mathrm{BrO_3^-} \rightarrow \mathrm{POM-complex} + \mathrm{Br^-} + 3\mathrm{H_2O}$$

The anti-interference ability is also usually considered as the key to evaluate the performance of the electrochemical sensors. Here, the CO_3^{2-}, HCO_3^{2}, SO_4^{2-}, Cl^- and Br^- as potential interference substances are introduced to investigate the anti-interference abilities of **1–3**-CPEs as electrochemical sensors in the process of detecting BrO_3^-. As shown in Fig. 7, the addition of BrO_3^- can lead to obvious current responses of the corresponding CPEs, but the response remained unchanged when the selected potential interference substances are added, indicating that **1–3**-CPEs as electrochemical sensors of BrO_3^- can exhibit excellent selectivity and anti-interference ability.

Catalytic oxidation of thioether

Generally, the POM-based complexes could usually be recognized as good catalysts for oxidation of thioether,[44,45] so the catalytic performances of complexes **1–3** for the oxidation of thioether were also studied here. The reaction of oxidation of methyl phenyl thioether (MPS) with **1** as catalyst and TBHP as oxidant was used to investigate the influences on the catalytic efficiencies of dosage of catalyst, reaction time, oxidant and temperature (Table 2). Firstly, the influence of reaction temperature is evaluated under the reaction condition containing 0.5 mmol substrate, 3 μmol catalysts and 0.75 mmol TBHP. Increasing the reaction temperature from room temperature to 50 °C, the conversion and selectivity reach to 99.5% and 98.6% within 40 minutes (Entries 1–3). When the temperature is raised to 60 °C, the conversion and selectivity are reduced to 99.0% and 96.3% (Entry 4), which reveals that the optimum reaction temperature is 50 °C.

Further, the changes of reaction time, dosage of catalyst and oxidants under the optimum reaction temperature lead to the decreases of conversion and selectivity (Entries 5–10). Meanwhile, the solvents such as ethanol, $CHCl_3$ and acetonitrile are appraised, indicating that methanol is satisfactory (Entries 11–13). So the most effective reaction condition is to use methanol as solvent under 50 °C within 40 minutes, with the suitable mole ratio of 1:1.5:0.6% for substrate, oxidate and catalyst, respectively.

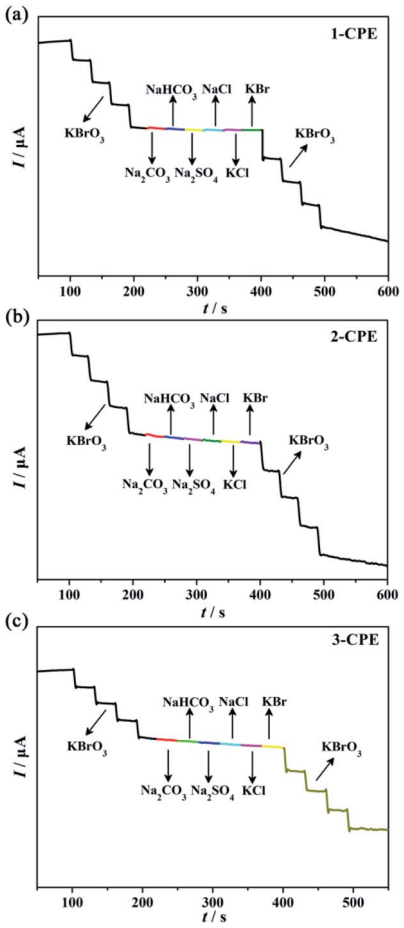

Fig. 7 Current responses of **1–3**-CPEs with the addition of BrO_3^- and interference substances.

The catalytic activities of **2** and **3**, as well as raw materials molybdate and $CrMo_6$ were further investigated under optimum condition, as shown in Table 3. When the complexes **2** and **3** are employed as catalysts, the excellent conversions and selectivity of 99.2% and 98.1% for **2**, 99.0% and 97.3% for **3**, can be obtained, which are comparable to the reported POM-based hybrids.[46–48] However, the use of $(NH_4)_6Mo_7O_{24}\cdot 4H_2O$ and $CrMo_6$ cause the lower conversions of 10.1% and 64.1%, despite the high selectivity of 90.9% and 91.4%. These results reveal that complexes **1–3** can show satisfying catalytic performances toward the oxidation of MPS to sulfoxide.

Further, the catalytic ability of **1** as a representative was estimated by choosing the thioether derivatives including these containing different groups and alkyl thioethers under the optimum condition. The results are summarized in Table 4. It can be observed that the conversions and selectivity of 4-methoxythioanisole, 4-chlorothioanisole and diphenylthioether due to the larger steric resistance are lower than that of MPS (Entries 2–4), but the conversions and selectivity are satisfactory or higher than that of MPS when the alkyl thioethers such as dipropyl thioether and 2-chloroethyl ethyl thioether are chosen (Entries 5 and 6). These results manifest that the steric hindrance of substrate play key influences on the conversion of thioether to sulfoxide in the presence of **1** as catalyst, which is similar to those reports.[49–51]

Considering that the recyclability and stability are very important to evaluate the catalytic performance of catalyst, the **1** as representative was also investigated by utilizing the reaction of MPS to sulfoxide under optimum condition (Fig. 8).

Table 3 Conversion and selectivity of MPS to sulfoxide by using different catalysts

Catalyst	Conv. (%)	Sel. (%)
1	99.5	98.6
2	99.2	98.1
3	99.0	97.3
$(NH_4)_6Mo_7O_{24}\cdot 4H_2O$	10.1	90.9
$CrMo_6$	64.1	91.4

Table 2 The influences on conversion and selectivity of reaction time, dosage of catalyst, oxidant, temperature and solvent in the presence of **1** as catalyst[a]

Entry	Catalyst (μmoL)	TBHP (mmoL)	Time (min)	Temp. (°C)	Conv. (%)[b]	Sel. (%)[c]
1	3	0.75	40	rt	81.5	91.1
2	3	0.75	40	40	99.1	97.0
3	3	0.75	40	50	99.5	98.6
4	3	0.75	40	60	99.0	96.3
5	3	0.75	30	50	78.5	99.5
6	3	0.5	40	50	91.0	99.2
7	3	None	40	50	<10	96.5
8	6	0.75	40	50	98.9	96.6
9	None	0.75	40	50	33.2	98.9
10	3[d]	0.75	40	50	98.0	84.0
11	3[e]	0.75	40	50	93.1	98.5
12	3[f]	0.75	40	50	87.8	97.4
13	3[g]	0.75	40	50	78.0	98.7

[a] Reaction condition: substrate (0.5 mmoL), methanol (2 mL), **1** (3 μmoL, 0.6 mol%). [b] Conversion and selectivity were analyzed by GC. [c] Conversion and selectivity were analyzed by GC. [d] H_2O_2. [e] Ethanol (2 mL). [f] $CHCl_3$ (2 mL). [g] Acetonitrile (2 mL).

Table 4 The conversion and selectivity of thioether derivatives to sulfoxides catalyzed by **1**

Entry	Substrate	Product	Conv. (%)	Sel. (%)
1			99.5	98.6
2			98.2	97.6
3			97.8	97.3
4	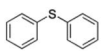		95.3	94.2
5		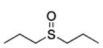	99.8	98.7
6			99.6	99.3

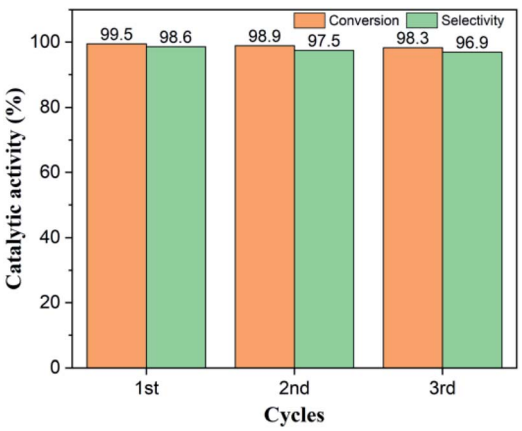

Fig. 8 Cyclic catalytic performance of **1** as catalyst for the oxidation of MPS.

The catalysts were filtered after catalytic reaction, and washed by using methanol, which were further reused to catalyze the oxidation of MPS to sulfoxide. After 3 runs, the catalytic ability of complex **1** has barely changed, and the conversion and selectivity remain still above 96%, indicating that the **1** as catalyst has good recyclability for the oxidation of MPS to sulfoxide. Furthermore, the stability of catalyst after catalytic reaction was assessed relying on PXRD (Fig. S5†), confirming the good stability of catalyst during the catalytic reaction.

Conclusions

In a word, three new POM-based complexes were prepared by using a bi-imidazole ligand containing carbazole connector. The metal centers and polyoxoanions play important roles in tuning the diverse architectures of the complexes. These complexes can be employed as the electrode materials for preparing the electrochemical sensors of BrO_3^- with lower LODs, likewise, as efficient catalysts for the oxidation of thioether to sulfoxide accompanying with satisfying recyclability and stability, which opens up a possible means for preparing novel POM-hybrids as electrochemical sensor and catalyst materials.

Conflicts of interest

There are no conflicts to declare.

Acknowledgements

The National Natural Science Foundation of China (No. 21771025, 21971024, 21671025) and the General Program Fund for Education Department of Liaoning Province (LJ2019004) are gratefully acknowledged.

Notes and references

1 M. Sadakane and E. Steckhan, *Chem. Rev.*, 1998, **98**, 219.
2 D. Jana, H. K. Kolli, S. Sabnam and S. K. Das, *Chem. Commun.*, 2021, **57**, 9910.
3 Y. Zou, H. Li, X. Zhao, J. Song, Y. Wang, P. Ma, J. Niu and J. Wang, *Dalton Trans.*, 2021, **50**, 12664.
4 C. Lee, D. Jeon, J. Park, W. Lee, J. Park, S. J. Kang, Y. Kim and J. Ryu, *ACS Appl. Mater. Interfaces*, 2020, **12**, 32689.
5 S. Herrmann, N. Aydemir, F. Nägele, D. Fantauzzi, T. Jacob, J. Travas-Sejdic and C. Streb, *Adv. Funct. Mater.*, 2017, **27**, 1700881.
6 J.-J. Chen, M. D. Symes, S.-C. Fan, M.-S. Zheng, H. N. Miras, Q.-F. Dong and L. Cronin, *Adv. Mater.*, 2015, **27**, 4649.
7 D. Pakulski, A. Gorczyński, W. Czepa, Z. Liu, L. Ortolani, V. Morandi, V. Patroniak, A. Ciesielski and P. Samorì, *Energy Storage Mater.*, 2019, **17**, 186.
8 S. G. Mitchell, C. Streb, H. N. Miras, T. Boyd, D.-L. Long and L. Cronin, *Nat. Chem.*, 2010, **2**, 308.
9 J. W. Jordan, G. A. Lowe, R. L. McSweeney, C. T. Stoppiello, R. W. Lodge, S. T. Skowron, J. Biskupek, G. A. Rance, U. Kaiser, D. A. Walsh, G. N. Newton and A. N. Khlobystov, *Adv. Mater.*, 2019, **31**, 1904182.
10 S. Maity, M. Je, B. R. Biradar, P. R. Chandewar, D. Shee, P. P. Das and S. S. Mal, *Energy Fuels*, 2021, **35**, 18824.
11 P. Mialane, C. Mellot-Draznieks, P. Gairola, M. Duguet, Y. Benseghir, O. Oms and A. Dolbecq, *Chem. Soc. Rev.*, 2021, **50**, 6152.
12 R. Yu, X.-F. Kuang, X.-Y. Wu, C.-Z. Lu and J. P. Donahue, *Coord. Chem. Rev.*, 2009, **253**, 2872.
13 C.-Y. Sun, S.-X. Liu, D.-D. Liang, K.-Z. Shao, Y.-H. Ren and Z.-M. Su, *J. Am. Chem. Soc.*, 2009, **131**, 1883.
14 X.-J. Yu, H. Zhong, Y.-M. Xian, Z.-P. Wang, S. Schneider, J. Scherr, T. Abu-Husein, Z. Zhang and A. Terfort, *Dalton Trans.*, 2020, **49**, 16627.
15 C. Zou, Z. J. Zhang, X. Xu, Q. H. Gong, J. Li and C. D. Wu, *J. Am. Chem. Soc.*, 2011, **134**, 87.
16 Y.-R. Wang, Q. Huang, C.-T. He, Y. Chen, J. Liu, F.-C. Shen and Y.-Q. Lan, *Nat. Commun.*, 2018, **9**, 4466.

17 Q. Huang, J. Liu, L. Feng, Q. Wang, W. Guan, L.-Z. Dong, L. Zhang, L.-K. Yan, Y.-Q. Lan and H.-C. Zhou, *Natl. Sci. Rev.*, 2019, **7**, 53.
18 C. Li, N. Mizuno, K. Yamaguchi and K. Suzuki, *J. Am. Chem. Soc.*, 2019, **141**, 7687.
19 A. Al-Yasari, P. Spence, H. El Moll, N. Van Steerteghem, P. N. Horton, B. S. Brunschwig, K. Clays and J. Fielden, *Dalton Trans.*, 2018, **47**, 10415.
20 V. S. V. Satyanarayana, P. G. Reddy and C. P. Pradeep, *RSC Adv.*, 2015, **5**, 59609.
21 L. Marleny Rodriguez-Albelo, A. R. Ruiz-Salvador, A. Sampieri, D. W. Lewis, A. Gómez, B. Nohra, P. Mialane, J. Marrot, F. Sécheresse, C. Mellot-Draznieks, R. Ngo Biboum, B. Keita, L. Nadjo and A. Dolbecq, *J. Am. Chem. Soc.*, 2009, **131**, 16078.
22 Y.-G. Lee, H. J. Lee and A. Jang, *Sens. Actuators, B*, 2017, **244**, 157.
23 H. B. Teh and S. F. Y. Li, *J. Chromatogr. A*, 2015, **1383**, 112.
24 M. R. Khan, S. M. Wabaidur, Z. A. Alothman, R. Busquets and M. Naushad, *Talanta*, 2016, **152**, 513.
25 H. M. Al-Saidi and M. S. El-Shahawi, *Spectrochim. Acta, Part A*, 2015, **138**, 736.
26 S. Li, B. Lu, J. Xin, L. Zhang, J. Pan, Y. Chen and X. Tan, *J. Solid State Chem.*, 2019, **278**, 120905.
27 B. R. Lu, S. B. Li, X. Z. Zhang, D. Q. Zhang, L. L. Fan, E. Y. Yan, Y. J. Zhang and L. Yu, *New J. Chem.*, 2019, **43**, 15804.
28 B. X. Dong, F. Y. Bu, Y. C. Wu, J. Zhao, Y. L. Teng, W. L. Liu and Z. W. Li, *Cryst. Growth Des.*, 2017, **17**, 5309.
29 X. L. Wang, Z. W. Cui, H. Y. Lin and Z. H. Chang, *CrystEngComm*, 2021, **23**, 2113.
30 L. Li, X. Wang, N. Xu, Z. H. Chang, G. C. Liu, H. Y. Lin and X. L. Wang, *CrystEngComm*, 2020, **22**, 8322.
31 L. Zhang, L. Chen, S. X. Liu, J. Gong, Q. Tang and Z. M. Su, *Dalton Trans.*, 2018, **47**, 105.
32 Y. N. Zhang, Y. Zhang, L. Li, J. L. Chen, P. Z. Li and W. H. Huang, *J. Electroanal. Chem.*, 2020, **861**, 113939.
33 G. G. Papagianni, D. V. Stergiou, G. S. Armatas, M. G. Kanatzidis and M. I. Prodromidis, *Sens. Actuators, B*, 2012, **173**, 346.
34 X. Wang, H. Li, J. Lin, C. Wang and X.-L. Wang, *Inorg. Chem.*, 2021, **60**, 19287.
35 G. M. Sheldrick, *SHELXS-2014, Program for Structure Solution*, University of Göottingen, Germany, 2014.
36 O. V. Dolomanov, L. J. Bourhis, R. J. Gildea, J. A. K. Howard and H. Puschmann, *J. Appl. Crystallogr.*, 2009, **42**, 339.
37 I. D. Brown and D. Altermatt, *Acta Crystallogr., Sect. B: Struct. Sci.*, 1985, **41**, 244.
38 X. Pan, X. L. Wang, X. Wang, Y. Li, G. C. Liu and H. Y. Lin, *CrystEngComm*, 2019, **21**, 6472.
39 M. L. Yang, S. Rong, X. M. Wang, H. Y. Ma, H. J. Pang, L. C. Tan, Y. X. Jiang and K. Q. Gao, *ChemNanoMat*, 2021, **7**, 299.
40 Y. L. Wang, Y. Y. Ma, Q. Zhao, L. Hou and Z. G. Han, *Sens. Actuators, B*, 2020, **305**, 127469.
41 B.-X. Dong, L. Chen, S. Y. Zhang, J. Ge, L. Song, H. Tian, Y. L. Teng and W. L. Liu, *Dalton Trans.*, 2015, **44**, 1435.
42 L. Chen, L. Tian, L. Liu, X. F. Tian, W. B. Song, H. D. Xu and X. H. Wang, *Sens. Actuators, B*, 2005, **110**, 271.
43 Y. C. Li, W. F. Bu, L. X. Wu and C. Q. Sun, *Sens. Actuators, B*, 2005, **107**, 921.
44 K. Liu, Z. X. Yao and Y.-F. Song, *Ind. Eng. Chem. Res.*, 2015, **54**, 9133.
45 X. R. Sun, J. Dong, Z. Li, H. F. Liu, X. T. Jing, Y. N. Chi and C. W. Hu, *Dalton Trans.*, 2019, **48**, 5285.
46 Y. Zhang, W.-D. Yu, B. Li, Z.-F. Chen and J. Yan, *Inorg. Chem.*, 2019, **58**, 14876.
47 Q. F. Xu, X. P. Sun, F. Hu, R. Wan, V. Singh, P. T. Ma, J. Y. Niu and J. P. Wang, *Materials*, 2017, **10**, 1173.
48 C. F. Pereira, F. Figueira, R. F. Mendes, J. Rocha, J. T. Hupp, O. K. Farha, M. M. Q. Simões, J. P. C. Tomé and F. A. A. Paz, *Inorg. Chem.*, 2018, **57**, 3855.
49 X.-S. Wang, Y.-B. Huang, Z.-J. Lin and R. Cao, *Dalton Trans.*, 2014, **43**, 11950.
50 D. J. Thompson, Y. Zhang and T. Ren, *J. Mol. Catal. A: Chem.*, 2014, **392**, 188.
51 J.-K. Li, J. Dong, C.-P. Wei, S. Yang, Y.-N. Chi, Y.-Q. Xu and C.-W. Hu, *Inorg. Chem.*, 2017, **56**, 5748.